BIOCHEMISTRY
including biophysical chemistry & molecular biology

Article

pubs.acs.org/biochemistry

Fluorescence Characterization of the Transfer RNA-like Domain of Transfer Messenger RNA in Complex with Small Binding Protein B

May Daher and David Rueda*

Department of Chemistry, Wayne State University, Detroit, Michigan 48202, United States

Supporting Information

ABSTRACT: Transfer messenger RNA (tmRNA) and small binding protein B (SmpB) are the main components of the trans-translation rescue machinery that releases stalled ribosomes from defective mRNAs. Little is known about how SmpB binding affects the conformation of the tRNA-like domain (TLD) of tmRNA. It has been previously hypothesized that the absence of a D stem in the TLD provides flexibility in the elbow region of tmRNA, which can be stabilized by its interaction with SmpB. Here, we have used Förster resonance energy transfer to characterize the global structure of the tRNA-like domain of tmRNA in the presence and absence of SmpB and as a function of Mg^{2+} concentration. Our results show tight and specific binding of SmpB to tmRNA. Surprisingly, our data show that the global conformation and flexibility of tmRNA do not change upon SmpB binding. However, Mg^{2+} ions induce an 11 Å compaction in the tmRNA structure, suggesting that the flexibility in the H2a stem may allow different conformations of tmRNA as the TLD and mRNA-like domain need to be positioned differently while moving through the ribosome.

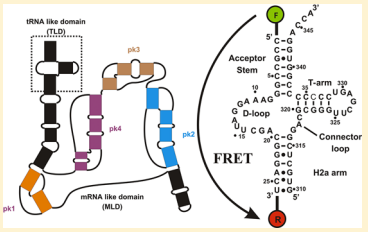

Defective or truncated mRNAs (mRNAs) lacking stop codons lead to ribosome stalling on the end of the message. Stalled ribosomes can cause two major problems for the cell: production of incomplete, nonfunctional and potentially toxic proteins and depletion of the ribosomal pool that is available for translation.[1,2] In bacteria, these problems can be solved by a rescue process called trans-translation, which employs the hybrid transfer mRNA (tmRNA) and its highly conserved cofactor, small binding protein B (SmpB).[3,4] These two factors are universally conserved in bacterial species, and trans-translation is important for a wide variety of physiological processes, including gene expression, pathogenesis, and response to stress, making tmRNA an attractive target for antibacterial drug discovery.[1,5] Indeed, Pyrazinamide, a first-line tuberculosis drug, acts by inhibiting the ribosome rescue pathway.[6]

Transfer mRNA consists of two domains (Figure 1A): the tRNA-like domain (TLD) and the mRNA-like domain (MLD). The TLD includes an acceptor stem and a TψC arm (Figure 1A,B). However, in lieu of a D arm, it contains an irregular D loop without predicted helical pairing, and instead of an anticodon loop, it contains an irregular helix (H2a) that joins the TLD to the MLD through four pseudoknots [pk1−pk4 (Figure 1A,B)]. The MLD comprises an open reading frame that encodes a protein tag that signals for degradation of the incomplete protein.[3,7−9] Transfer mRNA enters into the A site of stalled ribosomes with its TLD in complex with SmpB and the elongation factor EF-Tu.[3] In the A site, the nascent peptide chain is transferred to the TLD, which translocates into the P site releasing the defective mRNA. Then, the first codon of the MLD enters the decoding center, where it is translated by normal aminoacyl-tRNAs. The resulting peptide tag is recognized by specific cellular proteases that degrade the defective protein.[1,8,10] All of these steps require a special set of interactions among tmRNA, SmpB, the ribosome, and the translational cofactors.[11]

A transient electric birefringence (TEB) study of the tmRNA TLD in absence of SmpB has revealed a more obtuse angle (110° instead of 90°) between the acceptor and helix H2a stems compared to that in canonical tRNAs.[12] This has been confirmed in the crystal structure of the TLD−SmpB complex, which revealed an obtuse angle of 120° between the acceptor stem and helix H2a, but a 90° angle between the acceptor stem and SmpB.[13] On the basis of this result, the authors hypothesized that SmpB mimics a canonical acceptor stem and interacts with the decoding site, while the H2a arm functions as a class II tRNA long variable arm. More recently, interactions between SmpB and the decoding site have supported this hypothesis.[14,15]

It has previously been hypothesized that the lack of a D stem in the TLD may provide flexibility in the elbow region of tmRNA, between H2 and the acceptor arm, which can be stabilized by its interaction with SmpB.[16] This is an important question because it affects the possible tmRNA conformations during tmRNA accommodation and how the MLD is introduced into the decoding center while the aminoacyl group resides in the peptidyl transferase center. In particular, it is not yet known whether SmpB or Mg^{2+} ions modulate the TLD domain structure. To address this question, we have used fluorescence anisotropy and FRET to measure the distance between the acceptor and the H2a stem in the presence and absence of SmpB. We also compare our results to the features of a canonical tRNA and a mitochondrial tRNA (mtRNA) that lacks the D stem.

Received: November 27, 2011
Revised: April 4, 2012
Published: April 9, 2012

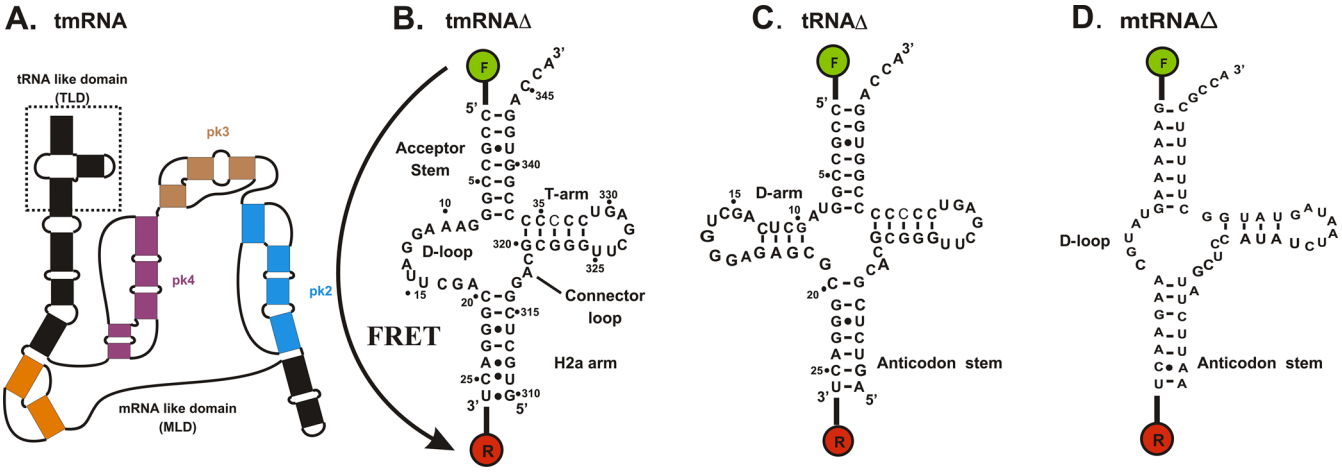

Figure 1. Secondary structure of tmRNA and the fluorophore-labeled constructs. (A) Secondary structure of tmRNA and location of the TLD and MLD. Four pseudoknots (pk1, orange; pk2, blue; pk3, brown; pk4, pink) connect the two major domains. (B–D) Fluorescein (F)- and tetramethylrhodamine (R)-labeled constructs for FRET studies: tmRNAΔ (B), tRNAΔ (C), and mtRNAΔ (D).

Surprisingly, our data show that the global conformation and flexibility of the TLD do not change upon SmpB binding. However, Mg^{2+} ions induce an 8 Å compaction of the TLD.

MATERIALS AND METHODS

RNA Purification and Fluorophore Labeling. RNA strands were purchased from the Keck Foundation Biotechnology Resource Laboratory at the Yale University School of Medicine (New Haven, CT). RNAs were constructed using two strands: a 5′ strand containing the D loop and a 3′ strand containing the T arm (sequences in Figure 1). The 5′ strands were labeled with a 5′ fluorescein and a 3′ amino linker (Figure 1). RNA strands were deprotected, purified, and labeled with a 3′ tetramethylrhodamine (TMR) as described previously.[17] The location of the fluorophores [top of the acceptor stem and bottom of helix H2a (Figure 1)] was set far from the SmpB binding site (elbow region) to minimize the possibility of affecting SmpB binding.

SmpB Expression and Purification. SmpB protein cloning and expression were performed as previously described.[16] The plasmid containing the *smpB* gene with a C-terminal histidine tag (pET21) was obtained from N. Ban (Institute of Molecular Biology and Biophysics, ETH, Zurich, Switzerland). The gene was transformed into *Escherichia coli* BL21/DE3. Histidine-tagged SmpB was bound to a nickel column (IMAC column), washed, and eluted with 250 mM imidazole [300 mM NaCl and 50 mM Na_2HPO_4 (pH 8.0)].[16] A 12% sodium dodecyl sulfate–acrylamide gel was used to check the protein purity. Pure fractions were dialyzed against storage buffer [20 mM NaCl and 10 mM Na_2HPO_4 (pH 6.5)]. The protein concentration was measured using UV–vis absorbance at 280 (extinction coefficient of 22900 M^{-1} cm^{-1}).

Anisotropy Measurements. Fluorescence anisotropy measurements were performed using a spectrofluorometer with automated polarizers (Varian, Cary Eclipse). Fluorescein-only labeled 5′ (25 nM) and 3′ (50 nM) strands were heated at 90 °C for 2 min and annealed for >15 min at room temperature in standard buffer [50 mM Tris-HCl (pH 7.5), 100 mM NaCl, and 1 mM $MgCl_2$]. Fluorescence anisotropy was studied in the presence of the donor fluorophore alone, because fluorescence energy transfer can result in a decrease in the donor fluorescence intensity, thus compromising our ability to measure fluorescence anisotropy and to interpret the results. Measurements were performed at room temperature at RNA:protein ratios varying from 1:0.0004 to 1:4. Fluorescein was excited at 490 nm (5 nm bandwidth); parallel ($I_{\|}$) and perpendicular ($I_{\perp}$) emission intensities were measured at 520 nm (5 nm bandwidth).[18−20] Fluorescence anisotropy was calculated as $r(t) = (I_{\perp} - GI_{\|})/(I_{\perp} + 2GI_{\|})$, where G is an empirically determined, instrument-dependent correction factor. The data were fit to the quadratic binding equation assuming 1:1 stoichiometry

$$f(\mathrm{SmpB}) = r_0 + (r_{\max} - r_0)\Big[K_D + [\mathrm{RNA}_0] + [\mathrm{SmpB}] - \sqrt{(K_D + [\mathrm{RNA}_0] + [\mathrm{SmpB}])^2 - 4[\mathrm{RNA}_0][\mathrm{SmpB}]}\Big] / (2[\mathrm{RNA}_0])$$

where r_0 and $r_{\max}$ are the fluorescence anisotropies of fluorescein-labeled tmRNAΔ alone and bound to SmpB, respectively, K_D is the dissociation constant, $[\mathrm{RNA}_0]$ is the initial RNA concentration (25 nM), and [SmpB] is the total (free plus bound) SmpB concentration. Control anisotropy experiments by direct excitation of TMR-labeled tmRNAΔ confirm that the binding affinity remains in the low nanomolar range and that neither the free amino linker nor TMR affects binding of SmpB to tmRNAΔ (Figure 1 of the Supporting Information).

Steady State Förster Resonance Energy Transfer (ssFRET) Measurements. FRET measurements were taken using a spectrofluorometer (Varian Cary Eclipse), as described previously.[17,21−24] Doubly labeled (Fluorescein and TMR) 5′ (25 nM) and 3′ (50 nM) strands were heated and annealed as described above. The experiments were performed at room temperature. Fluorescein was excited at 490 nm (10 nm bandwidth). Fluorescein and TMR emissions were measured at 520 and 580 nm (5 nm bandwidth), respectively. The apparent FRET efficiency was calculated as FRET = $I_{580}/(I_{580} + I_{520})$, where I_{520} and I_{580} are the fluorescein and TMR emission intensities, respectively. SmpB was titrated from 0.01 to 100 nM. For each measurement, the solution was manually mixed and allowed to incubate for 5 min before the emission spectra were recorded.

Time-Resolved FRET (trFRET) Measurements. To determine the end-to-end distance distribution of tmRNAΔ, we used trFRET, as described previously.[17,21,25] A 250 nM

dx.doi.org/10.1021/bi201751k | *Biochemistry* 2012, 51, 3531–3538

solution of labeled 5′ strand (labeled with only fluorescein or fluorescein and TMR) and 500 nM 3′ strand was heated and annealed as described above. Fluorescein was excited at 490 nm (30 nm bandwidth dichroic filter) with a Yb-doped fiber laser (5 ps pulses, 40 MHz). Donor emission was collected at 520 nm (20 nm bandwidth dichroic filter) using a microchannel photomultiplier tube (R3890U-52, Hamamatsu) feeding a time-correlated single-photon counting card (SPC-630, Becker & Hickl) under magic angle polarization (54.7°) to more than 40000 peak counts. Fluorescence decays were collected in 4816 channels with a time resolution of 12.2 ps/channel. A dilute nondairy coffee creamer solution was used to measure the instrument function. The decays of the donor emission in the absence and presence of the acceptor with and without SmpB were collected under identical conditions. The time resolved for the donor only complex was used to extract the three intrinsic parameters, donor lifetimes τ_i, fractional contributions α_i, and μ_i. The data from the doubly labeled tRNAΔs (I_{DA}) were then fit according to the following equation:

$$I_{DA}(t) = I_0 \int P(R) \sum_i \alpha_i \exp\left\{-\frac{t}{\tau_i}\left[1 + \left(\frac{R_0}{R}\right)^6\right]\right\} dR$$

where I_0 is the initial intensity, τ_i and α_i are the singly labeled lifetime and the corresponding decay amplitude, respectively, $P(R)$ is the distance distribution, and R_0 is the Förster distance for 50% energy transfer [independently determined for the fluorescein−TMR FRET pair for each construct (see the Supporting Information)].[17,21,25−27] The distance distribution $P(R)$ was analyzed as a three-dimensional weighted Gaussian:

$$P(R) = 4\pi R^2 N \exp[-(R - \mu)^2/\sigma^2]$$

where N is a normalization constant and σ and μ describe the shape of the Gaussian. An additional parameter was the fraction of singly labeled RNA because the labeling reaction could not be 100% efficient. The ability to quantify multiple populations, including singly labeled RNA, has been well established previously.[17,21,25−28] This equation provides information about the mean distance between the fluorescein and TMR; the distance distribution indicates the conformational flexibility of the complex, and the fractional population provides information about the basis for the thermodynamic analyses of the conformational equilibrium.[17,21] To test the effect of SmpB and Mg^{2+} on the fluorescein, we measured its quantum yield (QY) and the average excited lifetime for each fluorescein-only construct in the absence and presence of SmpB and in the absence and presence of Mg^{2+} (Supporting Information). The data show that, within the standard deviation, both the QY and the average excited state lifetime remain constant for all constructs under our conditions.

RESULTS

SmpB Binds tmRNAΔ Tightly and Specifically. First, we sought to confirm that SmpB efficiently binds the fluorophore-labeled tmRNAΔ construct using fluorescence anisotropy. Fluorescence anisotropy is a dimensionless quantity (r) that measures the rotation of a fluorophore. Low fluorescence anisotropies indicate that the fluorophore tumbles freely in solution, whereas high anisotropies indicate that the fluorophore rotation is hindered, for example, by the formation of a high-molecular weight complex.[19] In the absence of protein, the observed anisotropy value for tmRNAΔ alone is low (0.06 ± 0.01). In the presence of 100 nM SmpB, the anisotropy increases to 0.15 ± 0.03, indicating that a higher-molecular weight protein−RNA complex is formed. A protein titration from 0.01 to 100 nM (Figure 2) shows that the observed anisotropy values increase

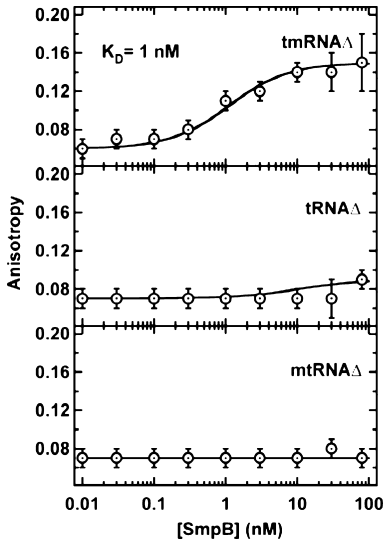

Figure 2. SmpB binds tmRNAΔ tightly and specifically. Binding isotherms [50 mM Tris-HCl (pH 7.5), 100 mM NaCl, and 1 mM $MgCl_2$] between SmpB and tmRNAΔ (top), tRNAΔ (middle), and mtRNAΔ (bottom). Anisotropy increases indicate binding of SmpB to the RNA. Only tmRNAΔ binds SmpB with a binding affinity (K_D) of 1.0 ± 0.1 nM.

smoothly from 0.06 to 0.15. A fit to the quadratic equation (see Materials and Methods) results in a dissociation constant (K_D) of 1.0 ± 0.1 nM, comparable to previously reported values.[8] This result shows that SmpB binds tightly to our fluorophore-labeled tmRNAΔ construct with a 1:1 stoichiometry.[8]

To test for the specificity of protein binding, we repeated the experiments using fluorophore-labeled alanyl tRNA [tRNAΔ (Figure 1)] and mitochondrial seryl tRNA [mtRNAΔ (Figure 1)], which are not expected to bind SmpB. The corresponding titrations show that the fluorescence anisotropy of both RNAs remains low (0.07 ± 0.01) throughout the protein concentration range, indicating that SmpB does not bind tRNAΔ or mtRNAΔ. These data are consistent with previous results that show that SmpB binds tRNA with a dissociation constant 400-fold higher than that of tmRNA.[8] Our data suggest that only one SmpB binds the TLD, in agreement with prior studies,[13,16] but in contradiction with one other study that suggests that multiple SmpB molecules can bind the TLD.[29]

Overall, the fluorescence anisotropy data show that SmpB binds tmRNAΔ tightly, specifically, and stoichiometrically.

Mg^{2+} but Not Na^+ Ions Inhibit SmpB Binding. We then sought to study the effect of monovalent and divalent cations on tmRNA−SmpB binding. We repeated the fluorescence anisotropy titration (Figure 2) in 0, 1, and 10 mM Mg^{2+} and in the presence of 20 or 100 mM Na^+. Figure 3 shows the resulting SmpB dissociation constants (K_D) under these conditions. In the absence of Mg^{2+} and in 100 mM Na^+, the dissociation constant is 0.4 ± 0.1 nM. Increasing the Mg^{2+} concentration to 1 and 10 mM increases the dissociation constant to 1.0 ± 0.1 and 2.6 ± 0.6 nM, respectively. These results show that Mg^{2+} ions have an inhibitory effect on SmpB binding.

When the sodium concentration is decreased to 20 mM (Figure 3, right panel), the binding dissociation constant ranges

dx.doi.org/10.1021/bi201751k | Biochemistry 2012, 51, 3531−3538

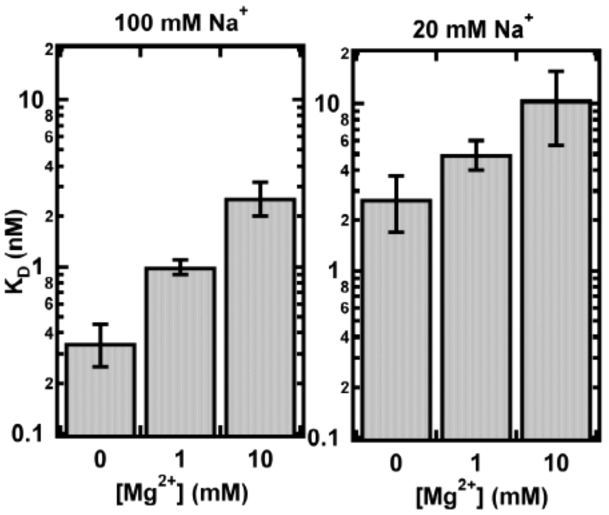

Figure 3. Magnesium ions have an inhibitory effect on SmpB binding. Binding affinities (K_D) of SmpB for tmRNAΔ as a function of Mg^{2+} and Na^+ concentrations. An increasing Mg^{2+} concentration causes a decrease in the SmpB binding affinity. A decreasing Na^+ concentration also decreases the SmpB binding affinity, and the Mg^{2+} effect becomes less pronounced. Error bars stem from three independent measurements.

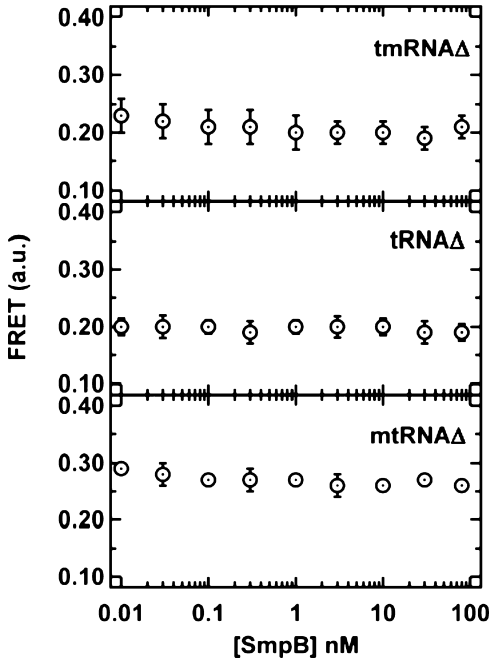

Figure 4. Global structure of tmRNAΔ that does not change upon SmpB binding. Apparent FRET efficiencies for the fluorophore-labeled tmRNAΔ (top), tRNAΔ (middle), and mtRNAΔ (bottom) as a function of SmpB concentration. Error bars are from three independent measurements. Apparent FRET efficiencies remain constant thoroughout the titration range, indicating that the global structure of tmRNAΔ does not change upon binding. Control RNAs (tRNAΔ and mtRNAΔ) are not expected to bind SmpB.

from 2.7 ± 1.0 nM (in the absence of Mg^{2+}) to 11 ± 5 nM (in 10 mM Mg^{2+}), between 4- and 8-fold higher than that in 100 mM Na^+. The fact that SmpB binds better at the higher concentration of Na^+ might be due to increased tmRNAΔ tertiary structural stability that in turn stabilizes SmpB binding. Regardless of the cause, this result shows that the Mg^{2+} inhibition of SmpB binding is specific and not solely electrostatic in nature. Overall, these results indicate that Mg^{2+} ions inhibit binding of SmpB to tmRNAΔ and that high Na^+ ion concentrations are required for tight SmpB binding.

SmpB Does Not Induce Global Conformational Changes in tmRNAΔ. To monitor the global structure of tmRNAΔ upon SmpB binding, we used steady state FRET (ssFRET), which measures the apparent efficiency of the transfer of energy from an excited donor fluorophore to a nearby acceptor fluorophore. The apparent FRET efficiency is extremely sensitive to the distance between the fluorophores in the 2−8 nm range; thus, FRET measurements can be a valuable tool for probing molecular structure and interactions.[30] We placed the fluorophores fluorescein and tetramethylrhodamine at the ends of the acceptor and helix H2a, respectively (Figure 1A), to detect any conformational changes that would alter the angle between the acceptor stem and the H2a arm. High FRET efficiency indicates that the two fluorophores are in the proximity of each other and, therefore, that a more acute angle exists between the helices, whereas low FRET efficiency indicates a longer distance between the two fluorophores and, therefore, a more obtuse angle between the helices. In the absence of SmpB, the observed apparent FRET efficiency is 0.23 ± 0.02 (Figure 4).

In the presence of 0.01−100 nM SmpB, the observed apparent FRET efficiency remains approximately constant, indicating that the global tmRNAΔ conformation remains unchanged. FRET can report on only the tmRNAΔ global conformation, and therefore, our experiments cannot rule out local conformational changes at the binding site of the protein. Control experiments with tRNAΔ and mtRNAΔ, which do not bind SmpB, also show no changes in the apparent FRET efficiency in the presence of 0.01−100 nM SmpB (Figure 4). Comparison of the observed FRET efficiencies reveals interesting structural differences among tmRNAΔ, tRNAΔ, and mtRNAΔ. The lowest observed apparent FRET efficiency (0.20 ± 0.02) corresponds to tRNAΔ, indicating that it has the longest distance between the acceptor stem and anticodon stem. The highest apparent FRET efficiency (0.28 ± 0.01) corresponds to mtRNAΔ, indicating that it has the shortest distance between the acceptor stem and anticodon stem. The tmRNAΔ apparent FRET efficiency (0.23 ± 0.02) lies between those. On the basis of the crystal structure and the TEB studies, one would expect tmRNAΔ to have a lower apparent FRET efficiency than tRNAΔ, in apparent contradiction with these results. A possible explanation is that the acceptor stem of tmRNAΔ rotates around its helical axis (relative to tRNAΔ) to bring the 5′ end closer to the H2a arm.

ssFRET provides only an average apparent FRET efficiency and may not detect the presence of minor populations in solution. To measure the distribution of distances between the acceptor stem and helix H2a in the tmRNAΔ−SmpB complex, we used time-resolved FRET (trFRET). trFRET consists of measuring the fluorescence lifetime of the donor fluorophore in the absence and presence of the acceptor (Figure 5, top left panel). The transfer of energy from the excited donor to the acceptor results in an apparent decrease in the donor fluorescence lifetime (compare the black and green curves), which can be used to determine the distribution of distances between the fluorophores (Figure 5, bottom left panel, green, and Materials and Methods). In the absence of SmpB, the resulting distribution for tmRNAΔ reveals a bimodal distribution. The major component (~70%, centered at 60 ± 1 Å) is assigned to the complex formed by the 5′ and 3′ strands, whereas the minor

dx.doi.org/10.1021/bi201751k | Biochemistry 2012, 51, 3531−3538

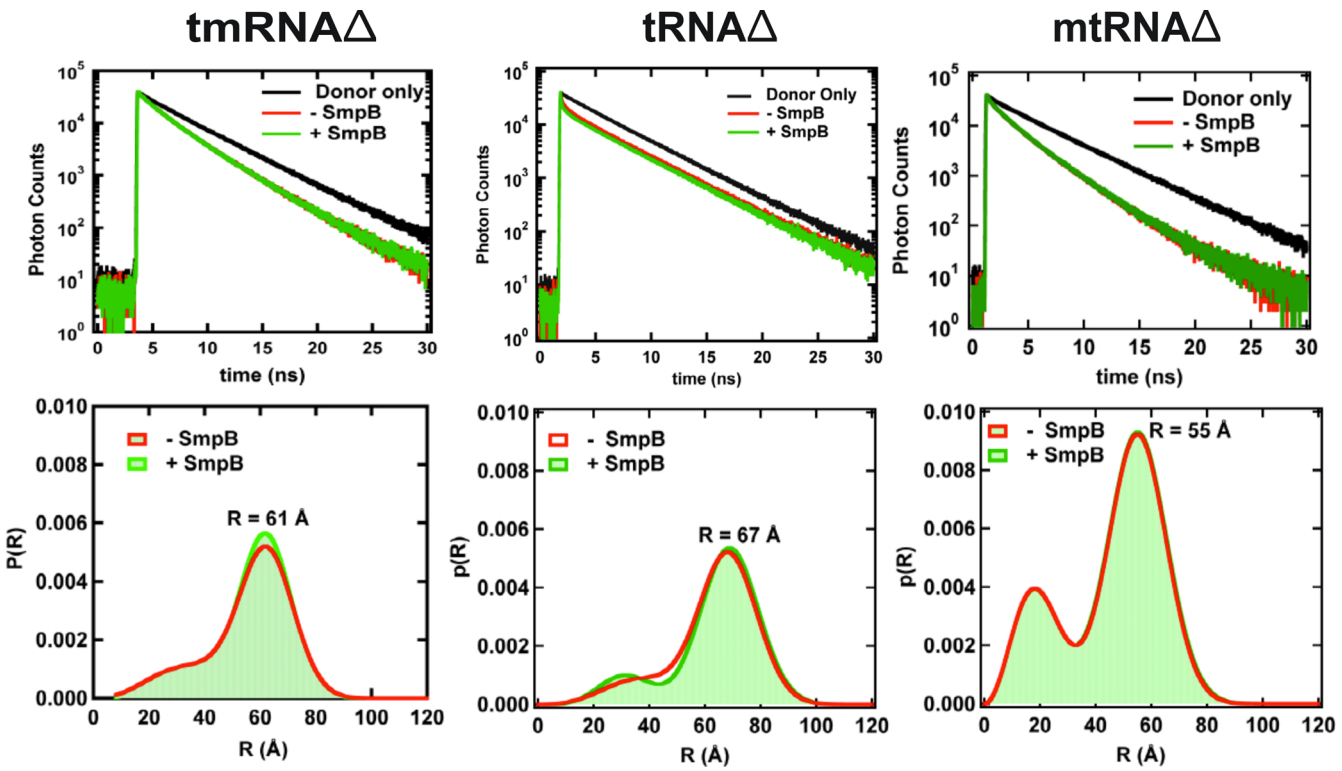

Figure 5. Donor fluorescence decays and resulting distance distributions. The top panels show the donor fluorescence decays in the absence (black) and presence (red) of acceptor and in the presence of SmpB (green) for tmRNAΔ, tRNAΔ, and mtRNAΔ, as indicated. The bottom panels shows the distance distributions calculated using Förster's equation (see Materials and Methods) in the absence (red) and presence (green) of SmpB. Results indicate that the global structure of tmRNAΔ does not change upon SmpB binding.

component (~30%, centered at 29 ± 1 Å) is assigned to a hairpin RNA formed by the 5′ strand alone. Control experiments in the absence of the 3′ strand (not shown) confirm these assignments. The bimodal distribution is confirmed by the reduced χ^2 ($\chi^2 \leq 1.2$) compared to a single distribution fit ($\chi^2 \geq 1.4$).[19,31] In the presence of SmpB, tmRNAΔ displays an almost identical distribution with a major component (~70%, centered at 61 ± 1 Å) and a minor component (~30%, centered at 29 ± 1 Å). This result confirms that the interaction between SmpB and tmRNAΔ does not change the distance between the acceptor stem and helix H2a of tmRNAΔ.

We repeated the experiments with the canonical tRNAΔ, which does not bind SmpB (Figure 5, top middle panel). The resulting distributions (bottom panel) show that, in the absence of SmpB (green), the major component is centered at 67 ± 1 Å, 7 Å longer than tmRNAΔ, in agreement with the ssFRET data (Figure 4). In the presence of SmpB (red), the major distribution remains unchanged, as expected. Similar results were observed with mtRNAΔ (Figure 5, right panels), except that the distance between the acceptor stem and the anticodon stem is ~6 Å shorter than that in tmRNAΔ, in agreement with the ssFRET data (Figure 4). Overall, these results show that SmpB does not change the overall conformation of tmRNAΔ upon binding. A comparison of the results for tmRNAΔ, tRNAΔ, and mtRNAΔ reveals that, in 1 mM Mg^{2+}, the distance distributions between the acceptor stem and helix H2a of tmRNAΔ lie between those observed for the control RNAs.

Mg^{2+} Ions Compress the tmRNAΔ Structure. To determine the effect of divalent ions on the global conformation of tmRNAΔ, we used trFRET to measure the distance distributions from the acceptor stem to H2a between 0.1 and 100 mM Mg^{2+} ions (Figure 6). In the absence of protein and in 0.1 mM Mg^{2+}, the mean distance between the two fluorophores is 62 ± 1 Å for tmRNAΔ (Figure 6A), 2 Å longer than in 1 mM Mg^{2+}. This distance decreases smoothly to reach 55 ± 1 Å at >10 mM Mg^{2+}. A fit to the quadratic equation yields a dissociation constant (K_{Mg}) of 2.2 ± 0.6 mM.

In the presence of SmpB and 0.1 mM Mg^{2+}, the distance between the two fluorophores is 64 ± 1 Å, 4 Å longer than in 1 mM Mg^{2+}. The distance also decreases with increasing magnesium concentrations to reach 55 ± 1 Å at >10 mM Mg^{2+} (Figure 6B). A fit to the quadratic equation also results in a dissociation constant (K_{Mg}) of 2.0 ± 0.9 mM. These results are within experimental error of the distance measured in the absence of SmpB, confirming that SmpB binding does not induce global conformational changes in tmRNAΔ upon binding. This result seems to be in apparent contradiction with our previous result showing that Mg^{2+} has an inhibitory effect on the binding site of the protein (Figure 2). However, previous studies have shown that Mg^{2+} ions have multiple binding sites with different binding affinities on tRNA.[32] Therefore, a possible explanation for this result is that two distinct Mg^{2+} ions are involved: one that has an inhibitor effect on the binding site of SmpB and the other that might bind inside the elbow region and results in the structural compaction of tmRNAΔ.

Unlike that in tmRNAΔ, the mean distance between the fluorophores in tRNAΔ remains constant at 67 ± 1 Å at all magnesium concentrations above 0.1 mM, suggesting that all Mg^{2+} ions are already tightly bound in the low concentration range. This is consistent with previous studies that showed that

dx.doi.org/10.1021/bi201751k | *Biochemistry* 2012, 51, 3531−3538

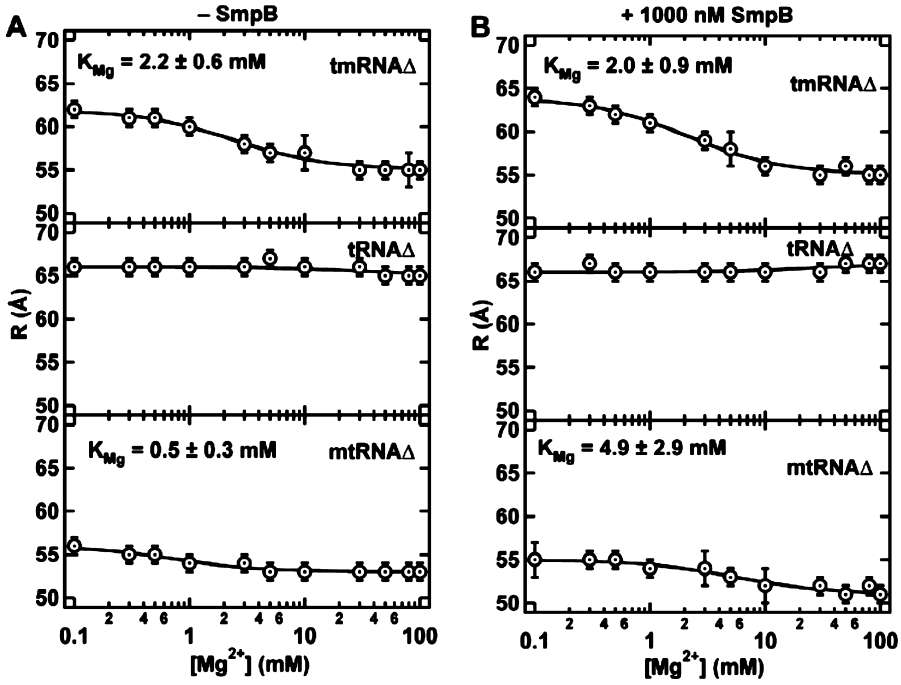

Figure 6. Magnesium ions compress the structure of tmRNAΔ. Donor−acceptor distance measurement for tmRNAΔ (top), tRNAΔ (middle), and mtRNAΔ (bottom) in the absence (left) and presence (right) of a saturating level of SmpB. A distance decrease is observed for tmRNAΔ and mtRNAΔ with increasing Mg^{2+} concentrations but not for tRNAΔ. Error bars are from three independent measurements. The data were fit to the quadratic equation (see Materials and Methods).

magnesium can stabilize tRNA tertiary structure in the micromolar range.[33] The presence of SmpB does not change the observed mean distance, as expected.

Mitochondrial tRNAΔ behaves like tmRNAΔ. In the absence of SmpB and at a low magnesium concentration, the observed mean distance is 56 ± 1 Å, and this decreases slightly to 53 ± 1 Å at >10 mM magnesium (Figure 6). A fit to the quadratic equation yields a dissociation constant (K_{Mg}) of 0.5 ± 0.3 mM, in agreement with a previously reported value.[34] This result suggests that the observed compaction for both tmRNAΔ and mtRNAΔ may be related to the absence of a D arm.

Overall, comparing the Mg^{2+} titration among tmRNAΔ, tRNAΔ, and mtRNAΔ suggests that the lack of a D stem (tmRNAΔ and mtRNAΔ) results in a low-millimolar affinity Mg^{2+} binding site that causes the distance between the acceptor stem and H2a to decrease but that does not compete for SmpB binding. Our data are in agreement with TEB data that showed a more acute angle in the presence of magnesium than in the absence of magnesium at 4 °C.[12]

DISCUSSION

Transfer messenger RNA and SmpB are two of the key components in the bacterial ribosome rescue system, and the interaction between these two molecules is necessary for entry into stalled ribosomes.[35] Previous studies have suggested that SmpB mimics the anticodon loop of canonical tRNA and binds to the decoding center of the ribosome, whereas the helix H2a functions as a long variable arm of class II tRNAs.[13,14] To determine the effect of SmpB and Mg^{2+} ion binding on the structure and dynamics of tmRNA, we designed a fluorophore-labeled construct (tmRNAΔ) that is very similar to the construct used in a previous crystallographic study.[16] The fluorescence anisotropy data confirm that SmpB binds tmRNAΔ tightly and specifically. We then used steady state and time-resolved FRET to monitor global conformational changes that would alter the angle between the acceptor stem and helix H2a of the tmRNAΔ upon interacting with SmpB. The results show no global conformational changes upon SmpB binding, suggesting that the angle between the acceptor step and helix H2a is more obtuse than that of canonical tRNAs, even in the absence of SmpB.

To fit into the ribosomal A site, canonical tRNAs must have a fixed distance between the decoding and peptidyl transferase centers, but our trFRET measurements show that, at saturating Mg^{2+} concentrations, the distance between the acceptor stem and helix H2a in tmRNAΔ is ∼11 Å shorter than in tRNAΔ in spite of the more obtuse angle (Figure 7A). Although a larger distance may be expected for tmRNA because of the larger angle, this result can be explained by rotation of the acceptor stem around the helical axis that brings the two ends closer to each other. Indeed, such a rotation is observed in the crystal structure of the TLD−SmpB complex (in Figure 7A, compare the left and middle panels).[13] The distance between the acceptor stem and the C-terminal domain of SmpB[13] matches very closely the distance between the acceptor stem and the anticodon stem of tRNA[36] (Figure 7A), consistent with the hypothesis that SmpB plays the role of the anticodon arm in tmRNA.[13−15]

Recent cryo-EM studies have shown a large conformational rearrangement taking place in the tmRNA structure while the first MLD codon interacts with the A site (Figure 7B).[37−39] These studies show that during accommodation helix H2 and pk1 move together toward the intersubunit space, while pk2 remains in place. This movement may assist in the placement of the region upstream of the open reading frame in contact with SmpB to position the resume codon into the A site of the stalled ribosome.[39] The Mg^{2+}-dependent conformational change observed here may correspond to the rearrangement observed in the cryo-EM studies, suggesting that the structure and flexibility

dx.doi.org/10.1021/bi201751k | *Biochemistry* 2012, 51, 3531−3538

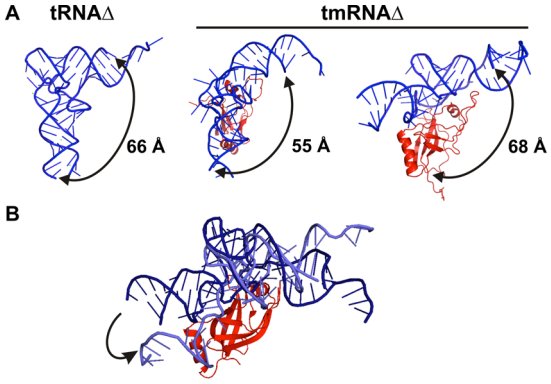

Figure 7. Comparison of distances in the model of the tmRNA−SmpB complex inside the stalled ribosome. (A) Measured distances between the acceptor stem and the anticodon stem in tRNAΔ and tmRNAΔ at saturating levels of Mg^{2+}. The ∼10 Å shorter distance in tmRNAΔ is consistent with the hypothesis that the H2a stem in tmRNA does not function as an anticodon stem mimic during trans-translation. On the basis of the crystal structure of the tmRNA−SmpB complex,[13] the distance between the acceptor stem and the C-terminus of SmpB matches well with tRNAΔ. (B) Cryo-EM studies reveal a large amplitude conformational change in tmRNA.[37−39] This image was generated using images of the TLD−SmpB complex in the accommodated (dark blue, Protein Data Bank entry 3IZ4) and translocated (light blue, Protein Data Bank entry 3IYQ) states. Only the tRNA-like domains are shown for the sake of clarity. The two structures were aligned using SmpB as the reference. The arrow shows the conformational change consistent with the Mg-induced compaction observed here.

of the H2 arm play an important role in tmRNA accommodation and translocation, perhaps in positioning pk1 and the MLD as the TLD moves through different sites in the ribosome. Altogether, our results may have interesting implications for the mechanism by which tmRNA replaces the defective mRNA with its own MLD.

■ ASSOCIATED CONTENT

Supporting Information

Quantum yield and R_0 for each construct, trFRET results, and average fluorescein excited state lifetimes. This material is available free of charge via the Internet at http://pubs.acs.org.

■ AUTHOR INFORMATION

Corresponding Author

*E-mail: david.rueda@wayne.edu. Telephone: (313) 577-6918. Fax: (313) 577-8822.

Funding

The Rueda lab is funded by the National Institutes of Health (R01GM085116) and a CAREER award from the National Science Foundation ([MCB0747285).

Notes

The authors declare no competing financial interest.

■ ACKNOWLEDGMENTS

We thank A. Buskirk for useful discussions and critically reading the manuscript, S. Atapattu, N. Ban for the pET21 plasmid, R. Lamichhane for overexpressing SmpB, E. Aléman for assistance with the trFRET measurements, and A. Brenlla for assistance with the determination of R_0.

■ ABBREVIATIONS

tmRNA, transfer mRNA; tmRNAΔ, truncated tmRNA derivative lacking nucleotides 83−326; tRNAΔ, truncated tRNA missing the anticodon loop; mtRNAΔ, truncated mitochondrial tRNA missing the anticodon loop; SmpB, small binding protein B; ssFRET, steady state Förster resonance energy transfer; trFRET, time-resolved Förster resonance energy transfer; TLD, tRNA-like domain; MLD, mRNA-like domain.

■ REFERENCES

(1) Keiler, K. C. (2008) Biology of trans-translation. *Annu. Rev. Microbiol. 62*, 133−151.

(2) Keiler, K. C. (2007) Physiology of tmRNA: What gets tagged and why? *Curr. Opin. Microbiol. 10*, 169−175.

(3) Dulebohn, D., Choy, J., Sundermeier, T., Okan, N., and Karzai, A. (2007) Trans-Translation: The tmRNA-Mediated Surveillance Mechanism for Ribosome Rescue, Directed Protein Degradation, and Nonstop mRNA Decay. *Biochemistry 46*, 4681−4693.

(4) Moore, S. D., and Sauer, R. T. (2007) The tmRNA system for translational surveillance and ribosome rescue. *Annu. Rev. Biochem. 76*, 101−124.

(5) Withey, J. H., and Friedman, D. I. (2003) A salvage pathway for protein structures: tmRNA and trans-translation. *Annu. Rev. Microbiol. 57*, 101−123.

(6) Shi, W., Zhang, X., Jiang, X., Yuan, H., Lee, J. S., Barry, C. E., III, Wang, H., Zhang, W., and Zhang, Y. (2011) Pyrazinamide inhibits trans-translation in *Mycobacterium tuberculosis*. *Science 333*, 1630−1632.

(7) Zwieb, C., Wower, I., and Wower, J. (1999) Comparative sequence analysis of tmRNA. *Nucleic Acids Res. 27*, 2063−2071.

(8) Karzai, A. W., Susskind, M. M., and Sauer, R. T. (1999) SmpB, a unique RNA-binding protein essential for the peptide-tagging activity of SsrA (tmRNA). *EMBO J. 18*, 3793−3799.

(9) Withey, J., and Friedman, D. (1999) Analysis of the role of trans-translation in the requirement of tmRNA for lambdaimmP22 growth in *Escherichia coli*. *J. Bacteriol. 181*, 2148−2157.

(10) Ivanova, N., Pavlov, M. Y., Felden, B., and Ehrenberg, M. (2004) Ribosome rescue by tmRNA requires truncated mRNAs. *J. Mol. Biol. 338*, 33−41.

(11) Himeno, H., Sato, M., Tadaki, T., Fukushima, M., Ushida, C., and Muto, A. (1997) In vitro trans translation mediated by alanine-charged 10Sa RNA. *J. Mol. Biol. 268*, 803−808.

(12) Stagg, S. M., Frazer-Abel, A. A., Hagerman, P. J., and Harvey, S. C. (2001) Structural studies of the tRNA domain of tmRNA. *J. Mol. Biol. 309*, 727−735.

(13) Bessho, Y., Shibata, R., Sekine, S., Murayama, K., Higashijima, K., Hori-Takemoto, C., Shirouzu, M., Kuramitsu, S., and Yokoyama, S. (2007) Structural basis for functional mimicry of long-variable-arm tRNA by transfer-messenger RNA. *Proc. Natl. Acad. Sci. U.S.A. 104*, 8293−8298.

(14) Nonin-Lecomte, S., Germain-Amiot, N., Gillet, R., Hallier, M., Ponchon, L., Dardel, F., and Felden, B. (2009) Ribosome hijacking: a role for small protein B during trans-translation. *EMBO Rep. 10*, 160−165.

(15) Miller, M. R., Liu, Z., Cazier, D. J., Gebhard, G. M., Herron, S. R., Zaher, H. S., Green, R., and Buskirk, A. R. (2011) The role of SmpB and the ribosomal decoding center in licensing tmRNA entry into stalled ribosomes. *RNA 17*, 1727−1736.

(16) Gutmann, S., Haebel, P. W., Metzinger, L., Sutter, M., Felden, B., and Ban, N. (2003) Crystal structure of the transfer-RNA domain of transfer-messenger RNA in complex with SmpB. *Nature 424*, 699−703.

(17) Lamichhane, R., Daubner, G. M., Thomas-Crusells, J., Auweter, S. D., Manatschal, C., Austin, K. S., Valniuk, O., Allain, F. H., and Rueda, D. (2010) RNA looping by PTB: Evidence using FRET and NMR spectroscopy for a role in splicing repression. *Proc. Natl. Acad. Sci. U.S.A. 107*, 4105−4110.

(18) Sevenich, F. W., Langowski, J., Weiss, V., and Rippe, K. (1998) DNA binding and oligomerization of NtrC studied by fluorescence anisotropy and fluorescence correlation spectroscopy. *Nucleic Acids Res. 26*, 1373−1381.
(19) Rueda, D., Hsieh, J., Day-Storms, J. J., Fierke, C. A., and Walter, N. G. (2005) The 5′ leader of precursor tRNAAsp bound to the *Bacillus subtilis* RNase P holoenzyme has an extended conformation. *Biochemistry 44*, 16130−16139.
(20) Walter, F., Putz, J., Giege, R., and Westhof, E. (2002) Binding of tobramycin leads to conformational changes in yeast tRNA(Asp) and inhibition of aminoacylation. *EMBO J. 21*, 760−768.
(21) Rueda, D., Wick, K., McDowell, S. E., and Walter, N. G. (2003) Diffusely bound Mg^{2+} ions slightly reorient stems I and II of the hammerhead ribozyme to increase the probability of formation of the catalytic core. *Biochemistry 42*, 9924−9936.
(22) Walter, N. G. (2001) Structural dynamics of catalytic RNA highlighted by fluorescence resonance energy transfer. *Methods 25*, 19−30.
(23) Rueda, D., and Walter, N. G. (2006) Fluorescent energy transfer readout of an aptazyme-based biosensor. *Methods Mol. Biol. 335*, 289−310.
(24) Gondert, M. E., Tinsley, R. A., Rueda, D., and Walter, N. G. (2006) Catalytic core structure of the trans-acting HDV ribozyme is subtly influenced by sequence variation outside the core. *Biochemistry 45*, 7563−7573.
(25) Eis, P. S., and Millar, D. P. (1993) Conformational distributions of a four-way DNA junction revealed by time-resolved fluorescence resonance energy transfer. *Biochemistry 32*, 13852−13860.
(26) Walter, N. G., Burke, J. M., and Millar, D. P. (1999) Stability of hairpin ribozyme tertiary structure is governed by the interdomain junction. *Nat. Struct. Biol. 6*, 544−549.
(27) Pereira, M. J., Harris, D. A., Rueda, D., and Walter, N. G. (2002) Reaction pathway of the trans-acting hepatitis delta virus ribozyme: A conformational change accompanies catalysis. *Biochemistry 41*, 730−740.
(28) Hsieh, J., Koutmou, K. S., Rueda, D., Koutmos, M., Walter, N. G., and Fierke, C. A. (2010) A divalent cation stabilizes the active conformation of the *B. subtilis* RNase P × pre-tRNA complex: A role for an inner-sphere metal ion in RNase P. *J. Mol. Biol. 400*, 38−51.
(29) Wower, J., Zwieb, C. W., Hoffman, D. W., and Wower, I. K. (2002) SmpB: A protein that binds to double-stranded segments in tmRNA and tRNA. *Biochemistry 41*, 8826−8836.
(30) Walter, N. (2003) Probing RNA Structural Dynamics and Function by Fluorescence Resonance Energy Transfer (FRET). *Curr. Protoc. Nucleic Acid Chem.*, 11.10.1−11.10.23.
(31) Klostermeier, D., and Millar, D. P. (2001) Time-resolved fluorescence resonance energy transfer: A versatile tool for the analysis of nucleic acids. *Biopolymers 61*, 159−179.
(32) Bolton, P. H., and Kearns, D. R. (1977) Effect of cations on tRNA structure. *Biochemistry 16*, 5729−5741.
(33) Romer, R., and Hach, R. (1975) tRNA conformation and magnesium binding. A study of a yeast phenylalanine-specific tRNA by a fluorescent indicator and differential melting curves. *Eur. J. Biochem. 55*, 271−284.
(34) Jones, C. I., Spencer, A. C., Hsu, J. L., Spremulli, L. L., Martinis, S. A., DeRider, M., and Agris, P. F. (2006) A counterintuitive Mg^{2+}-dependent and modification-assisted functional folding of mitochondrial tRNAs. *J. Mol. Biol. 362*, 771−786.
(35) Saguy, M., Gillet, R., Metzinger, L., and Felden, B. (2005) tmRNA and associated ligands: A puzzling relationship. *Biochimie 87*, 897−903.
(36) Sussman, J. L., Holbrook, S. R., Warrant, R. W., Church, G. M., and Kim, S. H. (1978) Crystal structure of yeast phenylalanine transfer RNA. I. Crystallographic refinement. *J. Mol. Biol. 123*, 607−630.
(37) Weis, F., Bron, P., Giudice, E., Rolland, J. P., Thomas, D., Felden, B., and Gillet, R. (2010) tmRNA-SmpB: A journey to the centre of the bacterial ribosome. *EMBO J. 29*, 3810−3818.
(38) Weis, F., Bron, P., Rolland, J. P., Thomas, D., Felden, B., and Gillet, R. (2010) Accommodation of tmRNA-SmpB into stalled ribosomes: A cryo-EM study. *RNA 16*, 299−306.
(39) Fu, J., Hashem, Y., Wower, I., Lei, J., Liao, H. Y., Zwieb, C., Wower, J., and Frank, J. (2010) Visualizing the transfer-messenger RNA as the ribosome resumes translation. *EMBO J. 29*, 3819−3825.